# Transverse and polarization effects in index-guided vertical-cavity surface-emitting lasers

M. S. Torre*
*Instituto de Física Arroyo Seco, Universidad Nacional del Centro de la Provincia de Buenos Aires, Pinto 399 (7000) Tandil, Argentina*

C. Masoller†
*Departament de Fisica i Enginyeria Nuclear, Universitat Politecnica de Catalunya, Colom 11, E-08222 Terrassa, Spain*

Paul Mandel‡
*Université Libre de Bruxelles, Optique Nonlinéaire Théorique, Campus Plaine C. P. 231, B-1050 Bruxelles, Belgium*
(Received 23 May 2006; published 11 October 2006)

We study numerically the polarization dynamics of vertical-cavity surface-emitting lasers (VCSEL's) operating in the fundamental transverse mode. We use an extension of the spin-flip model that not only accounts for the vector nature of the laser field, but also considers spatial transverse effects. The model assumes two orthogonal, linearly polarized fields, which are coupled to two carrier populations, associated with different spin sublevels of the conduction and valence bands in the quantum-well active region. Spatial effects are taken into account by considering transverse profiles for the two polarizations, for the two carrier populations, and for the carrier diffusion. The optical profile is the $LP_{01}$ mode, suitable for describing index-guided VCSEL's with cylindrical symmetry emitting on the fundamental transverse mode for both polarizations. We find that in small-active-region VCSEL's, fast carrier diffusion induces self-sustained oscillations of the total laser output, which are not present in larger-area devices or with slow carrier diffusion. These self-pulsations appear close to threshold, and, as the injection current increases, they grow in amplitude; however, there is saturation and the self-pulsations disappear at higher injection levels. The dependence of the oscillation amplitude on various laser parameters is investigated, and the results are found to be in good qualitative agreement with those reported by Van der Sande *et al.* [Opt. Lett. **29**, 53 (2004)], based on a rate-equation model that takes into account transverse inhomogeneities through an intensity-dependent confinement factor.

DOI: 10.1103/PhysRevA.74.043808 PACS number(s): 42.55.Px, 42.60.Mi, 42.65.Sf

## I. INTRODUCTION

Due to the important improvements that have been made in their performance capabilities, vertical-cavity surface-emitting lasers (VCSEL's) are nowadays employed in a wide range of practical applications, such as optical communications and data storage systems. VCSEL's have a very short cavity (typically of a few wavelengths of the emitted light) and thus they operate in a single longitudinal mode. They have a circular beam profile, which is desirable for optimal coupling into optical fibers; they have very low threshold currents and can be modulated at high speeds; they are compact and can be integrated in large two-dimensional arrays. However, they have two important drawbacks: they usually exhibit polarization and transverse-mode instabilities [1].

In conventional edge-emitting lasers the rectangular transverse section geometry and waveguiding effects lead to emission of linearly polarized light with stable polarization locked onto a fixed axis. In VCSEL's, due to the circular symmetry of the transverse section, the polarization is not fixed by geometrical constraints but rather by residual fabrication anisotropies, and VCSEL's emit light linearly polarized along one of two orthogonal directions, usually associated with crystalline orientation or stress. When the VCSEL begins to lase, one linear polarization dominates and, as the injection current is increased, in many devices it is observed that the emission switches to the orthogonal linear polarization, a phenomenon referred to as polarization switching (PS). The PS is usually accompanied by complex polarization dynamics in which there is either polarization coexistence (simultaneous emission on both of the orthogonal linear polarizations with different emission frequencies), polarization hopping (noise-induced competition between the two orthogonal linear polarizations with different emission frequencies), or emission of elliptically polarized light (on both orthogonal linear polarizations with the same emission frequency) [2–6]. In addition, fundamental mode emission is not maintained for increasing drive current, and higher-order transverse modes emerge, usually with a polarization that is orthogonal to that of the fundamental mode [1].

It is important to fully understand the polarization and transverse-mode behavior VCSEL's, and considerable attention has been given to elucidate the mechanisms determining the polarization selection at threshold and the polarization switching for increasing injection under single and multi-transverse-mode operation [7–16]. Material birefringence is a key ingredient that results in (i) a frequency split between the two polarizations (in the range of a few to about 50 GHz) and (ii) different transverse confinements of the two polarizations (i.e., different overlap with the gain region). It is then expected that spatial hole burning and carrier diffusion

*Electronic address: marita@exa.unicen.edu.ar
†URL: http://www.fisica.edu.uy/~cris. Electronic address: cristina.masoller@upc.edu
‡URL: http://www.ulb.ac.be/sciences/ont/en.html. Electronic address: pmandel@ulb.ac.be

 

can have a strong influence on the polarization of the emitted light.

Moreover, spatial hole burning and carrier diffusion also lead to waveguiding effects, which can result in self-pulsations of the total output upon increasing the laser drive current. The mechanism is well known in edge-emitting lasers: the spatial hole burning depletes the carrier density in the center of the active region, increasing the refractive index. As a result, the mode is more efficiently confined with increasing power, and there is an enhancement of the effective modal gain that can give rise to self-sustained oscillations. As the drive current is increased further there is saturation (because the carrier density cannot be depleted below the transparency value), and the self-pulsations eventually disappear at high-output powers.

In VCSEL's, self-pulsations have been experimentally observed by Willemsen *et al.* [17] and explained theoretically by several authors [18,20,21]. Scire *et al.* [18] proposed a mechanism based on the interplay of saturable gain and saturable absorption. They consider that the VCSEL-active region is surrounded by an unpumped cladding region that acts as an absorbing region. Using the framework of the spin-flip rate-equation model, the absorbing region was taken into account through an additional carrier reservoir (as in the Yamada model [19]). Carrier diffusion was incorporated in the rate equations through terms coupling the populations in the active and absorbing regions. Depending on the birefringence and on the laser drive current, four qualitatively different behaviors were found: stable linearly polarized output, intensity pulsations with stable polarization, pulsations of both, the total intensity and the two orthogonal polarizations, and polarization self-pulsation with nearly constant (total) output. Panajotov *et al.* [20] proposed an alternative mechanism, also capable of inducing self-pulsations, based on waveguiding effects. Using a effective-index self-consistent dynamical model, Panajotov *et al.* showed that self-pulsations can appear due to an interplay between the carrier-induced antiguiding and the index guiding (either the built-in index guiding in oxide-confined VCSEL's or the thermally induced index guiding in proton-implanted VCSEL's). In both cases the waveguiding is improved during the leading edge of the optical pulse because of carrier depletion and is worsened on the tail of the optical pulse because of the restoration of the carrier density. Van der Sande *et al.* [21] proposed a rate-equation model to take into account waveguiding effects through an intensity-dependent transverse confinement factor, which was calculated within the weakly guided approximation, assuming a core refractive index that depends on the modal intensity profile. This model predicts self-pulsations of the laser output, which are in good agreement with those observed experimentally and with those occurring in the spatiotemporal effective-index dynamical model.

The aim of the present contribution is to provide further insight into spatial hole burning and carrier diffusion effects in VCSEL's. In previous work [22–24] we studied this subject using a model for multi-transverse-mode VCSEL's first proposed by Valle *et al.* [8]. The model is applicable to index-guided VCSEL's such that the optical profile is fixed by the built-in index step, therefore allowing a description in terms of modal amplitudes of various transverse modes [25]. This model takes into account spatial hole burning and carrier diffusion but not the polarization of the emitted light. Here, we combine the spatiotemporal model of Valle *et al.* with the spin-flip rate equations [9,10] for describing the polarization dynamics of VCSEL's, following the approach previously proposed by Martin-Regalado *et al.* [26]. The spin-flip model considers two orthogonal, linearly polarized fields, coupled to two carrier populations, associated with different spin sublevels of the conduction and valence bands in the quantum-well-active region. In [26], transverse profiles for the orthogonal polarizations and for the two carrier populations were incorporated to the model. For index-guided VCSEL's, the optical profiles and frequencies were fixed, determined by the built-in refraction index step as in the model of Valle *et al.*; for gain-guided VCSEL's, the optical profiles were determined dynamically from Maxwell-Bloch equations including diffraction.

The main focus of this work is the influence of spatial effects—namely, spatial hole burning and carrier diffusion—on index-guided VCSEL's. Section II presents the model and a summary of the results previously reported in [26]. Section III presents numerical simulations showing that in small-active-region VCSEL's, fast carrier diffusion induces self-sustained oscillations of the total laser output. These oscillations are not present either in larger-area devices or with slow carrier diffusion. We study the influence of relevant parameters on the amplitude and the frequency of the self-pulsations, varying the active region area, the carrier diffusion rate, and the sweep rate of the current ramp. A comparison is made with experimental observations, as well as with the predictions of other models. Section IV contains a summary of the results and the conclusions.

## II. THE MODEL

The model takes into account slowly varying complex amplitudes of left- and right-circular polarizations $E_+$ and $E_-$ coupled to two carrier populations $N_+$ and $N_-$ with opposite spins [10]. The equations can be written in terms of the complex amplitudes of two orthogonal linear polarizations $E_x=(E_++E_-)/\sqrt{2}$ and $E_y=-i(E_+-E_-)/\sqrt{2}$. Assuming single-transverse-mode and single-longitudinal-mode emission in both polarizations, the optical field is written as

$$\mathbf{E}(\mathbf{r},z,t)=[E_x(t)\psi_x(\mathbf{r})\mathbf{x}+E_y(t)\psi_y(\mathbf{r})\mathbf{y}]e^{i(\beta z-\omega t)}+\text{c.c.}, \quad (1)$$

where $\psi_x(\mathbf{r})$ and $\psi_y(\mathbf{r})$ are the transverse profiles, $\beta=k\eta$ is the reference propagation constant ($\beta L=q\pi$, where $L$ is the longitudinal extent of the laser cavity and $q$ is an integer), $k$ is the light wave number in vacuum, $\eta$ is the effective background refractive index, $\omega=ck$ is the associated frequency, and $c$ is the velocity of light in vacuum.

In the framework of the index-guided approximation, the transverse profiles $\psi_x(\mathbf{r})$ and $\psi_y(\mathbf{r})$ are determined by the built-in refractive index step between the active core region and the surrounding cladding region, and are solutions of the Helmholtz equation. Because of the transverse circular geometry of the VCSEL, $\psi_x$ and $\psi_y$ can be expressed more conveniently in cylindrical coordinates $r$ and $\theta$:

$$\psi_{x,y}(\mathbf{r}) = R_{x,y}(r)\cos(m_{x,y}\theta), \tag{2}$$

where $m_{x,y}$ are integers that determine the azimuthal variation and the radial parts $R_{x,y}(r)$ are the solutions of [27]:

$$r^2\frac{d^2R_x}{dr^2} + r\frac{dR_x}{dr} + [(k_0^2n_x^2 - \beta^2)r^2 - m^2]R_x = 0,$$

$$r^2\frac{d^2R_y}{dr^2} + r\frac{dR_y}{dr} + [(k_0^2n_y^2 - \beta^2)r^2 - m^2]R_y = 0, \tag{3}$$

where $k_0=\omega/c$ is the free space wave number and $n_x$ ($n_y$) is the refractive index corresponding to the $x$ ($y$) polarization. Birefringence is taken into account assuming that the refractive index in the core region in the $x$ direction, $n_x^{core}$, and in the $y$ direction, $n_y^{core}$, are different, while in the cladding region $n^{clad}$ is isotropic [26]:

$$n_{x,y}(r) = n_{x,y}^{core} \text{ for } r \le a,$$

$$n_{x,y}(r) = n^{clad} \text{ for } r > a, \tag{4}$$

where $a$ is the radius of the core region. The solutions of Eq. (3) are

$$R_{x,y}(r) = E_{x,y}\frac{J_m(u_{x,y}r/a)}{J_m(u_{x,y})} \text{ for } r \le a,$$

$$R_{x,y}(r) = E_{x,y}\frac{K_m(wr/a)}{K_m(w)} \text{ for } r > a, \tag{5}$$

where $J_m$ and $K_m$ are Bessel functions of the first and second kind, respectively, and

$$u_{x,y} = a[(k_0n_{x,y}^{core})^2 - \beta^2]^{1/2},$$

$$w = a[\beta^2 - (k_0n^{clad})^2]^{1/2} \tag{6}$$

are dimensionless parameters. Continuity at $r=a$ gives

$$\frac{u_{x,y}J_m'(u_{x,y})}{J_m(u_{x,y})} = \frac{wK_m'(w)}{K_m(w)}, \tag{7}$$

which is known as the characteristic equation for the linearly polarized (LP) modes [27]. For each longitudinal mode there is a set of solutions, $k_0=k_{mn}$, referred to as the $LP_{mn}$ modes of the $q$th longitudinal mode (the first subscript on LP refers to the $m$ azimuthal value and the second subscript corresponds to the various roots for that $m$ value). Because of birefringence, $n_x^{core}$ and $n_y^{core}$ are slightly different, and therefore, the $x$ and $y$ polarizations have different transverse confinements: the $LP_{mn}^{x,y}$ profiles are not degenerate and one polarization is better confined than the other. In addition, the two polarizations have different free-space wave vectors $k_{0x}$ and $k_{0y}$ and a frequency split of

$$\omega_y - \omega_x = c(k_{0y} - k_{0x}). \tag{8}$$

In the following, we assume that the laser emits on the fundamental transverse mode $LP_{01}$ in both polarizations (this has the advantage of reducing the computation time because the profiles have azimuthal symmetry). The profiles are normalized such that $\int_0^\infty \psi_{x,y}^2(r)rdr=1$.

The equations for the complex amplitudes $E_x$ and $E_y$, the total population density, $N=N_++N_-$, and the population difference, $n=N_+-N_-$, are [26]

$$\frac{dE_x}{dt} = k(1+i\alpha)[(G_x-1)E_x + ig_{xy}E_y] - (\gamma_a + i\gamma_p)E_x + \sqrt{\beta_{sp}}\xi_x(t), \tag{9}$$

$$\frac{dE_y}{dt} = k(1+i\alpha)[(G_y-1)E_y - ig_{xy}E_x] + (\gamma_a + i\gamma_p)E_y + \sqrt{\beta_{sp}}\xi_y(t), \tag{10}$$

$$\frac{\partial N}{\partial t} = \mu + D\frac{\partial^2 N}{\partial r^2} - \gamma_N[N(1 + |E_x|^2\psi_x^2 + |E_y|^2\psi_y^2) + in(E_yE_x^* - E_xE_y^*)\psi_x\psi_y], \tag{11}$$

$$\frac{\partial n}{\partial t} = -\gamma_s n + D\frac{\partial^2 n}{\partial r^2} - \gamma_N[n(|E_x|^2\psi_x^2 + |E_y|^2\psi_y) + iN(E_yE_x^* - E_xE_y^*)\psi_x\psi_y]. \tag{12}$$

Here $k$ is the field decay rate, $\gamma_N$ is the decay rate of the total carrier population, $\gamma_s$ is the decay rate of the population difference (which accounts for the mixing of carrier populations with different spins), $\alpha$ is the linewidth enhancement factor, $D$ is the diffusion coefficient, $\beta_{sp}$ is the spontaneous emission strength, $\xi_{x,y}$ are uncorrelated Gaussian white noises with zero mean, and $\mu$ is the normalized injection current (the threshold current is at $\mu=1$ neglecting transverse inhomogeneities). The injection is uniform over the transverse area of the core region (disk contact) and is zero outside: $\mu(r,t)=j(t)$ for $r\le a$, $\mu(r,t)=0$ for $r>a$ and $j(t)$ allows for the generation of current ramps.

The gain terms are given by the overlap of the transverse profiles with the carrier density:

$$G_x(t) = \int_0^\infty N(r,t)\psi_x^2(r)rdr, \tag{13}$$

$$G_y(t) = \int_0^\infty N(r,t)\psi_y^2(r)rdr, \tag{14}$$

$$g_{xy}(t) = \int_0^\infty n(r,t)\psi_x(r)\psi_y(r)rdr. \tag{15}$$

Due to birefringence the two polarizations have slightly different transverse profiles, and therefore, they have different modal gains. This can result in a polarization-selection mechanism at threshold, as discussed below.

The parameter $\gamma_a$ is the dichroism parameter that accounts for an *external* gain or loss anisotropy, which is not due to the different overlap of the transverse profiles with the active region, but which arises due to imperfections in the fabrication process. The parameter $\gamma_p$ is the birefringence parameter that accounts for the frequency splitting of the two polarizations, $\gamma_p=(\omega_y-\omega_x)/2$, and is calculated from Eq. (8). We

remark that in this model $\gamma_p$ is not a free parameter: the polarization with the larger (core) refractive index (i.e., the better confined) is the one with the lower emission frequency.

In the absence of anisotropies ($\gamma_a=0$, $\gamma_p=0$) the solutions of the model are linearly polarized states with arbitrary orientation of the polarization [9]. When cavity anisotropies are included, the solutions are two orthogonal linearly polarized and two elliptically polarized states [10]. Their stability depends on the gain-to-loss ratios of the two polarizations, the birefringence, and the saturable dispersion of the material. In certain parameter regions a linear stability analysis predicts a polarization switching for varying injection. Moreover, hysteresis occurs when the injection current is first increased and then decreased [10], in good agreement with many experimental observations.

The type of polarization switching that occurs for increasing injection depends on several parameters. Let us summarize some results of previous studies [10,26]. To fix ideas, we assume that the $x$ polarization is the better confined polarization ($n_x^{core}>n_y^{core}$) and, therefore, has the lower frequency ($\gamma_p>0$).

In the absence of external gain anisotropies ($\gamma_a=0$), if birefringence is large enough, modal gain differences determine the polarization selection at threshold: the better-confined $x$ polarization always turns on at threshold. However, for low birefringence, modal gain differences are not large enough to fix the polarization, and there is bistability at threshold. In this case, if $\gamma_p<\gamma_s/2\alpha$, when the $x$ polarization turns on at threshold the model predicts for increasing injection current a PS to the $y$ polarization. This PS, from the low-frequency (high-modal-gain) $x$ polarization to the high-frequency (low-modal-gain) $y$ polarization, has been referred to as type-II [28–30] and has been explained, in the context of this model, in terms of the interplay of birefringence, saturable dispersion, and spin-flip processes [10]. The PS from the high-frequency (low-modal-gain) $y$ polarization to the low-frequency (high-modal-gain) $x$ polarization, type-I PS, does not occur if $\gamma_a=0$ because (i) for low birefringence there is bistability at threshold, and if the $y$ polarization turns on at threshold, it remains stable as the injection increases; (ii) for large birefringence, the $y$ polarization does not turn on because the better confined $x$ polarization is selected at threshold. To summarize, in the framework of the spin-flip model (SFM) model extended to account for transverse inhomogeneities, in order to observe type-I PS, some amount of external gain anisotropy, which benefits the lesser-confined $y$ polarization ($\gamma_a>0$), must be included. In this case, a type-I PS can occur for increasing injection if the birefringence is large enough (if $\gamma_p>\gamma_s/2\alpha$ [26]).

In the next section we study these two types of PS, focusing on the influence of the area of the core region and of carrier diffusion.

## III. NUMERICAL RESULTS

We simulated the model equations with typical VCSEL parameters indicated in Table I. The parameters are the same as used in previous studies [10,26], but it is worth remarking that in [10,26] spontaneous emission noise was not taken into account, and as mentioned in the Introduction, noise can also induce polarization hopping in the polarization bistability region [4]. Since we want to focus on transverse effects, we try to avoid noise-induced switching and therefore we use a value of $\beta_{sp}$ that is not too large to induce switching, but that is still realistic, as it was shown in [31] that it is adequate to describe the polarization-resolved intensity noise of VCSEL's operating in the fundamental transverse mode.

TABLE I. Parameters used in the VCSEL simulation.

| Value | Parameter | Description |
|---|---|---|
| 8 | $q$ | Cavity resonance number |
| 1 $\mu$m | $L$ | Length of the active region |
| 3, 5 $\mu$m | $a$ | Radius of the active region |
| 3.5, 3.498 | $n_y^{core}$, $n^{clad}$ | Refractive indices |
| 3 | $\alpha$ | Linewidth enhancement factor |
| 300 ns$^{-1}$ | $k$ | Field decay rate |
| 1 ns$^{-1}$ | $\gamma_N$ | Carrier recombination rate |
| 50 ns$^{-1}$ | $\gamma_s$ | Spin-flip rate |
| $10^{-5}$ ns$^{-1}$ | $\beta_{sp}$ | Spontaneous emission rate |
| 0.3,5.0 $\mu$m$^2$/ns | $D$ | Carrier diffusion rate |

In order to study type-I and type-II PS we consider two sets of parameters ($\gamma_a$, $\gamma_p$): for $\gamma_a$ large enough, the $y$ polarization is selected at threshold, and if birefringence is also large ($\gamma_p>\gamma_s/2\alpha$), a PS to the $x$ polarization (type-I PS) occurs for increasing injection; for $\gamma_a=0$, when the $x$ polarization turns on at threshold, if birefringence is not too large ($\gamma_p<\gamma_s/2\alpha$), a PS to the $y$ polarization (type-II PS) occurs for increasing injection. Indeed, as discussed in the previous section, if $\gamma_a=0$, there is bistability at threshold; thus, if the $y$ polarization turns on, no PS occurs. The birefringence parameter $\gamma_p$ is varied by modifying $n_x^{core}$ while keeping $n_y^{core}$ and $n^{clad}$ fixed. The influence of the laser transverse section area is analyzed by considering various values of the core radius $a$ ($a$ is small enough to be consistent with the assumption of fundamental transverse mode operation in both polarizations). The influence of carrier diffusion is analyzed varying the diffusion coefficient $D$. Typical values corresponding to slow and fast diffusion are $D=0.3$ and 5.0 $\mu$m$^2$/ns, respectively.

### A. Analysis of the polarization-resolved *L-I* curve

To study the polarization-resolved $L$-$I$ curve, the injection current was varied linearly, from $\mu_{ini}=0.8$ to $\mu_{end}=2.8$ in a time interval $\Delta T$ ($\Delta T=200$ ns unless otherwise stated).

Figures 1 and 2 display the influence of carrier diffusion in type-I PS (Fig. 1) and in type-II PS (Fig. 2), when the active region radius is $a=5$ $\mu$m. We plot $I_x=|E_x|^2$, $I_y=|E_y|^2$, and $I_t=I_x+I_y$ for slow carrier diffusion in Figs. 1(a) and 2(a), and for fast carrier diffusion in Figs. 1(b) and 2(b). It can be observed that carrier diffusion slightly increases the injection current at which the laser turns on ($\mu_{th}=1$ in the absence of transverse inhomogeneities) and also increases the injection current at which the PS occurs. This is expected because

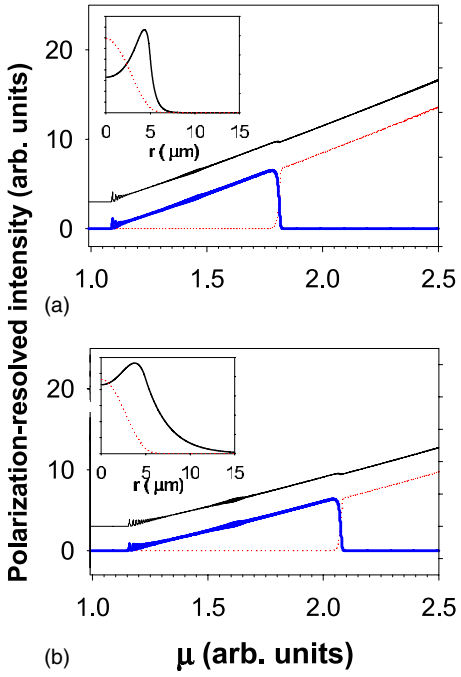


FIG. 1. (Color online) Influence of carrier diffusion on type-I PS from the $y$ polarization (thick line, blue) to the $x$ polarization (dotted line, red). The black line indicates the total intensity (shifted vertically for clarity). $a=5$ $\mu$m, $\gamma_a=2$ ns$^{-1}$, and $n_x^{core}=3.500181$, which gives $\gamma_p=44.34$ GHz (a) $D=0.3$ $\mu$m$^2$/ns and (b) $D=5$ $\mu$m$^2$/ns. The inset displays the optical profile (dotted line) and the carrier profile (solid line) at $\mu=2.5$.

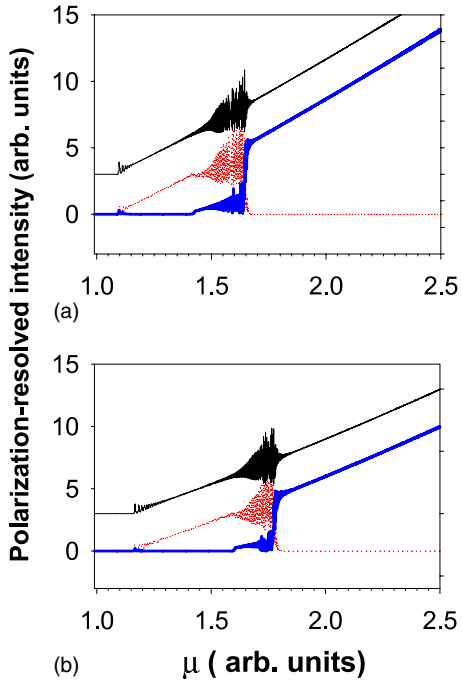


FIG. 2. (Color online) Influence of carrier diffusion on type-II PS. $a=5$ $\mu$m, $\gamma_a=0$, and $n_x^{core}=3.5000181$, which gives $\gamma_p=4.5$ GHz (a) $D=0.3$ $\mu$m$^2$/ns and (b) $D=5$ $\mu$m$^2$/ns.

diffusion diminishes the current effectively injected into the active region of the laser. The insets in Figs. 1(a) and 1(b) display the optical and carrier transverse profiles: for slow diffusion there is a pronounced spatial hole burning (SHB) and few carriers are in the cladding region; for fast carrier diffusion the SHB effect is less pronounced and the population of carriers in the cladding region is larger. While type-I PS is abrupt, type-II PS is accompanied by oscillations of the total intensity and of the intensities of the two polarizations. These oscillations are not due to transverse inhomogeneities because they are also present in the rate-equation model [10].

In a smaller-area laser, fast carrier diffusion not only increases the threshold and PS points, but also induces self-sustained oscillations of the total intensity, regardless of the polarization state, as shown in Fig. 3(b) for type-I PS and in Fig. 4(b) for type-II PS. For comparison, Figs. 3(a) and 3(b) display the $L$-$I$ curve for the same radius and slow carrier diffusion. We observe that the polarization switching does not seem to affect the oscillations. The self-pulsations appear near threshold, as undamped relaxation oscillations, their amplitude grows as the injection current increases, and then there is saturation with the oscillations disappearing at higher injection levels. These self-pulsations are not present in the rate-equation model [10] and therefore are due to transverse inhomogeneities. Similar self-pulsations have been observed in an extension of the SFM model where the absorbing unpumped region surrounding the central gain region is modeled as an additional carrier reservoir [18] and in models that do not consider polarization effects, but only waveguiding effects (in the form of an intensity-dependent transverse confinement factor [21] or in the form of thermal lensing due to heat-induced refractive index change and carrier-induced antiguiding [20]).

The duration of the current ramp, $\Delta T$, is another key parameter determining the polarization-resolved $L$-$I$ curve. The

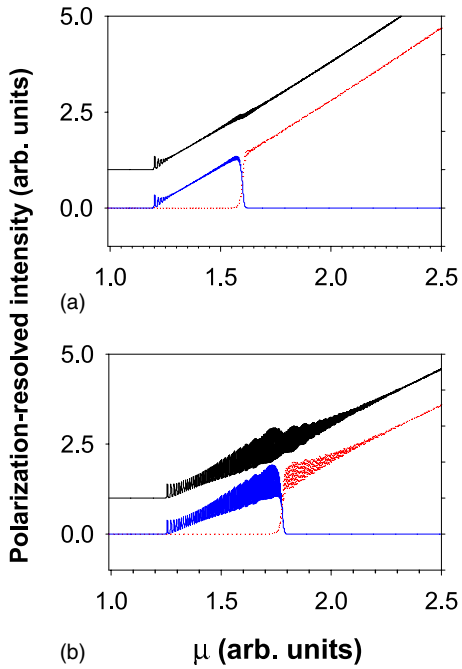


FIG. 3. (Color online) Influence of carrier diffusion on type-I PS for $a=3$ $\mu$m, other parameters as in Fig. 1. (a) $D=0.3$ $\mu$m$^2$/ns and (b) $D=5$ $\mu$m$^2$/ns.

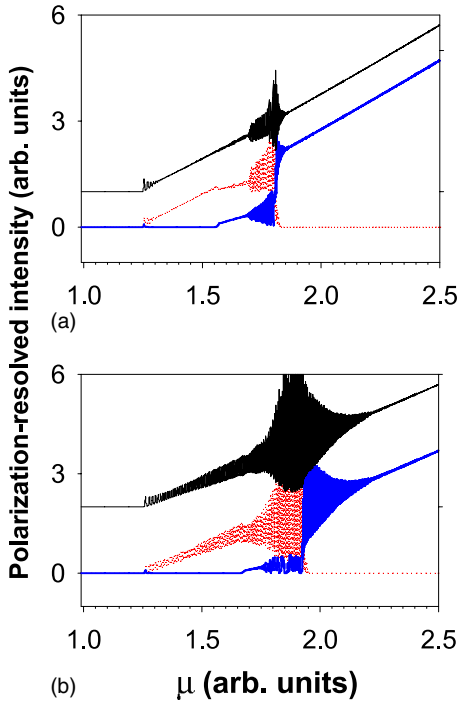


FIG. 4. (Color online) Influence of carrier diffusion on type-II PS for $a=3$ $\mu$m, other parameters as in Fig. 2. (a) $D=0.3$ $\mu$m$^2$/ns and (b) $D=5$ $\mu$m$^2$/ns.

region of self-pulsations excitation depends on the duration of the current ramp (Fig. 5), suggesting a more abrupt disappearance of the oscillations with slower ramps (in good agreement with the bifurcation analysis of the rate-equation model; see Fig. 2 of [21]). When carrier diffusion is slower (Fig. 6), fast current ramps delay the PS point to higher injection levels. This is expected as the same effect is observed in the SFM rate-equation model [32].

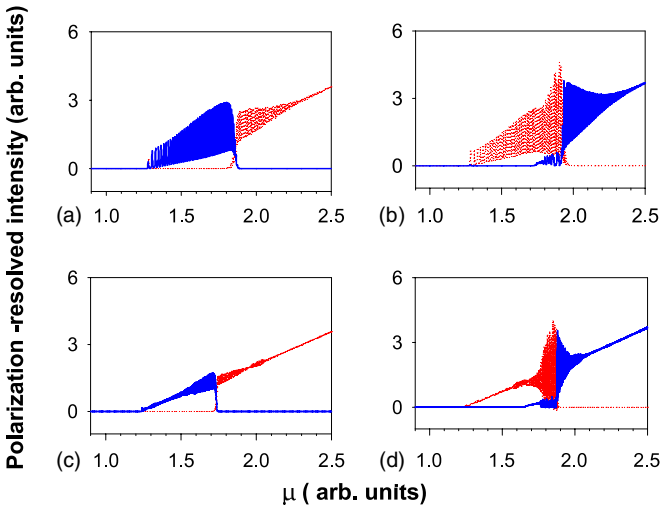


FIG. 5. (Color online) Influence of the duration of the current ramp, for fast carrier diffusion. $D=5$ $\mu$m$^2$/ns, $a=3$ $\mu$m. (a), (c) Type-I PS. (b), (d) Type-II PS. (a), (b) Fast current ramp: $\Delta T=100$ ns. (c), (d) Slow current ramp: $\Delta T=500$ ns.

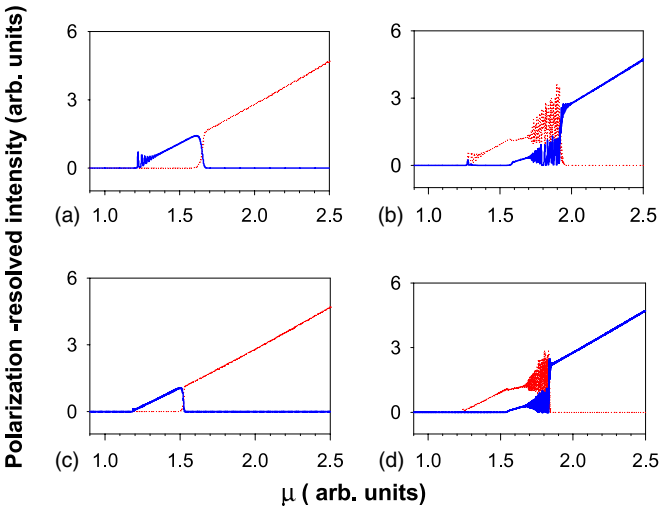


FIG. 6. (Color online) Influence of the duration of the current ramp, for slow carrier diffusion. $D=0.3$ $\mu$m$^2$/ns, all other parameters as in Fig. 5.

### B. Analysis of the self-pulsations

In this section we analyze the dependence of the amplitude and frequency of the oscillations on various laser parameters: the radius of the transverse area, $a$, the diffusion coefficient $D$, and the injection current $\mu$. Other parameters are fixed as in Fig. 1.

The intensity time traces for two values of the transverse area radius and various values of the injection current are shown in Fig. 7. If the radius $a$ is not too small (left column of Fig. 7), the self-pulsations are sinusoidal over the entire range of injection currents; their amplitude first grows and then decreases with the injection. For a smaller transverse area (right column of Fig. 7) we observe regular pulses that grow in amplitude with increasing injection, and there is also saturation at high values of $\mu$.

A plot of the self-pulsation amplitude versus the injection current for fixed $D$ and various values of $a$, Fig. 8(a), reveals a strong dependence of the amplitude on $a$. This dependence can be expected because in small-aperture VCSEL's the modal overlap with the cladding region increases, thus resulting in stronger saturable absorption. These features are in good qualitative agreement with the results presented in [21], based on a rate-equation model that takes into account transverse inhomogeneities through an intensity-dependent transverse confinement factor. A plot of the frequency squared versus the injection current, Fig. 8(b), reveals that when $a$ is not too small, the relation is linear (indicating undamped relaxation oscillations), but as the transverse area decreases, the role saturable absorption in the unpumped cladding region increases and the relation $f^2$ vs $\mu$ is nonlinear.

In our model the parameter determining the disappearance of the self-pulsation at high injection currents due to saturation is $\mu a^2$: when plotting the amplitude and the frequency squared versus $\mu a^2$, Fig. 9, it can be observed that the oscillations occur in the parameter range $\mu a^2 \lesssim 15$ $\mu$m$^2$, and the relation $f^2$ vs $\mu$ is nonlinear in this parameter region.

Another parameter that affects the self-pulsations is the diffusion coefficient: the larger the value of $D$, the larger the

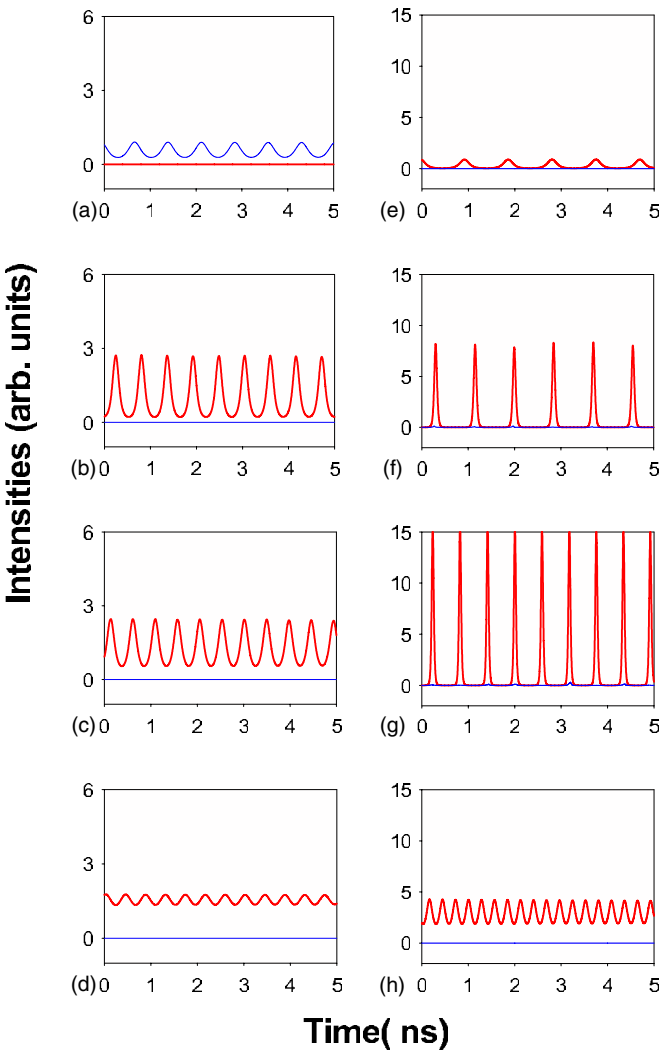


FIG. 7. (Color online) Time traces of the $y$ polarization (thin line, blue) and the $x$ polarization (thick line, red) for various values of the injection current. $D=5\ \mu m^2/ns$. Left column: $a=3\ \mu m$ and (a) $\mu=1.41$, (b) 1.6, (c) 1.7, and (d) 1.8. Right column: $a=2.3\ \mu m$ and (e) $\mu=1.45$, (f) 1.7, (g) 2.1, and (g) 2.8. Since we keep the values of $n_x^{core}$, $n_y^{core}$, and $n^{clad}$ fixed, there is a variation of the birefringence parameter: $\gamma_p=41.24$ GHz for $a=2.3$ and $\gamma_p=47.73$ GHz for $a=3.0$. Other parameters as in Fig. 1.

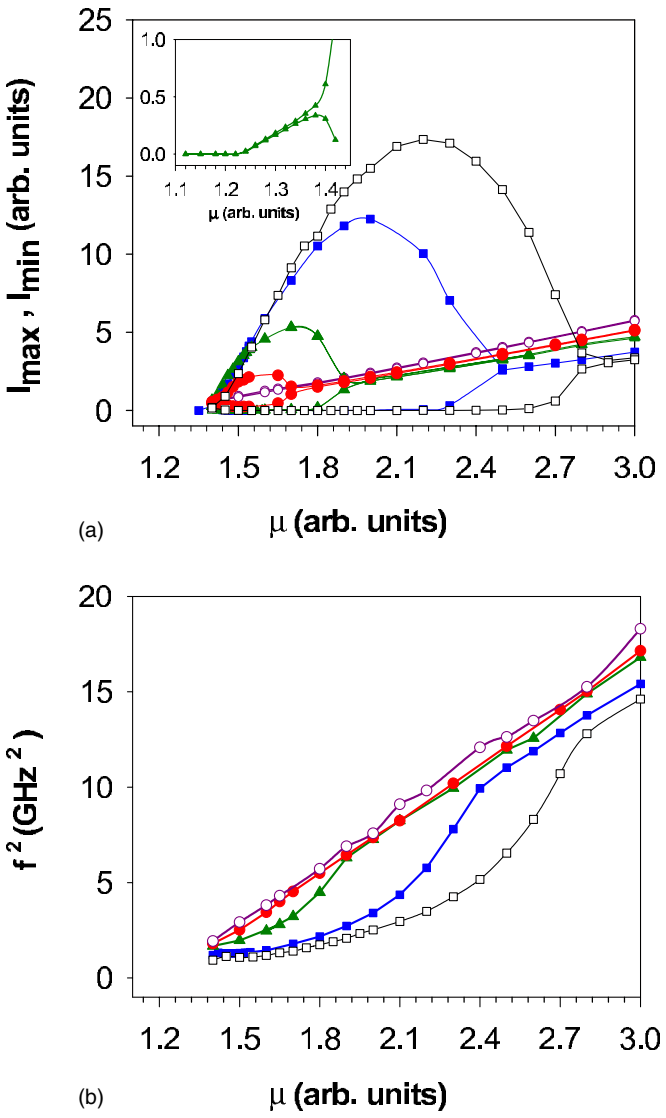


FIG. 8. (Color online) Influence of the transverse area size. (a) Amplitude and (b) frequency squared of the total intensity oscillations vs the injection current for $D=5\ \mu m^2/ns$ and various values of the transverse area radius: $a=2.3\ \mu m$, open squares; $a=2.5\ \mu m$, solid squares; 2.8 $\mu m$, triangles; 3 $\mu m$, solid circles; and 3.2 $\mu m$, open circles. The inset shows that the oscillations emerge slightly above threshold.

oscillation amplitude, as shown in Fig. 10(a). A plot of the frequency squared versus injection, Fig. 10(b), shows that for slow diffusion the relation is linear, indicating that the oscillations are linked to undamped relaxation oscillation, in agreement with the experimental observations of Refs. [17,33]. For larger $D$, saturation effects in the unpumped cladding region result in a nonlinear relation.

## IV. CONCLUSIONS

We studied the dynamics of VCSEL's within the framework of a spatially dependent spin-flip model. The fundamental $LP_{01}$ transverse mode of a weakly guiding cylindrical waveguide was used to describe the transverse profile of two orthogonal linear polarizations. Birefringence was taken into account by considering different core refractive indices for the two polarizations. This leads to a relation between the transverse confinement and the frequency split between the two polarizations, the better-confined mode having the lower frequency.

The influence of carrier diffusion and the transverse area size were analyzed. We found that the polarization-resolved $L$-$I$ curve strongly depends on these parameters. Small transverse area and fast carrier diffusion give rise to self-sustained pulsations, while larger area and/or slower diffusion are favorable to stable operation. The influence of the current ramp sweep rate was also analyzed. With slow carrier diffusion the sweep rate has the same effect as in the spatially independent rate-equation model [32]: fast ramps delay the PS point to higher injection values. With fast carrier diffusion, the region

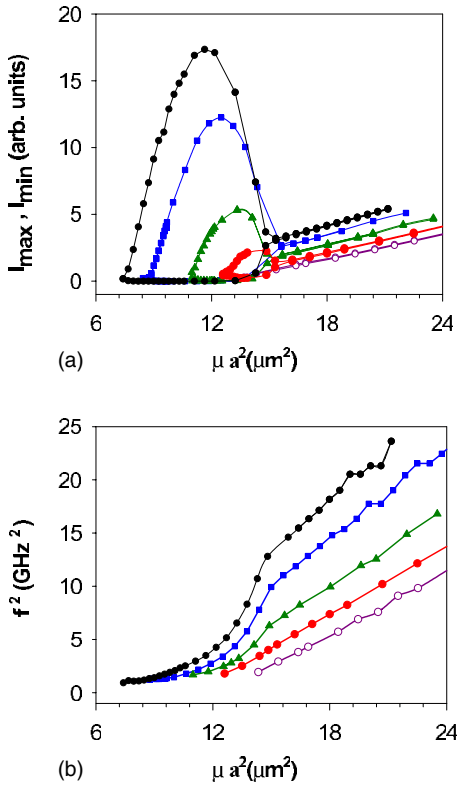


FIG. 9. (Color online) Amplitude and frequency squared of the oscillations vs $\mu a^2$. Parameters are the same as in Fig. 8.

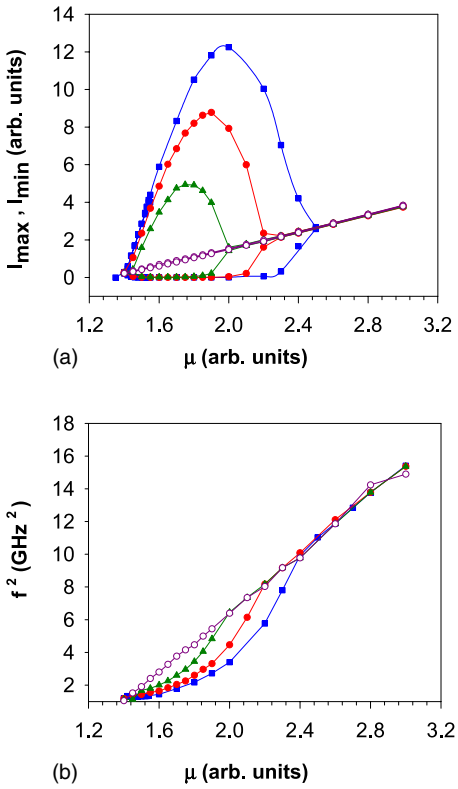


FIG. 10. (Color online) Influence of carrier diffusion. (a) Amplitude and (b) frequency squared of the total intensity oscillations vs the injection current for $a=2.5$ $\mu$m and various values of the diffusion coefficient: $D=3$ m$^2$/ns, circles; 4 m$^2$/ns, triangles; 4.5 m$^2$/ns, dots; and 5 m$^2$/ns, squares.

of excitation of self-pulsations depends on the sweep rate: the amplitude is smaller and they disappear more abruptly with slower ramps. We characterized the influence of transverse effects on the self-pulsations, analyzing the dependence of their amplitude and frequency with the diffusion coefficient and the transverse area size. We found that if the transverse area is not too small (roughly speaking, $a>3$ $\mu$m) and the carrier diffusion is not too fast (roughly speaking, $D<3$ $\mu$m$^2$/ns), the self-pulsations are sinusoidal over the entire range of injection currents, and their frequency squared varies linearly with the injection, suggesting that the oscillations are undamped relaxation oscillations. With smaller radius or faster diffusion, saturation in the cladding region leads to pulsing behavior, and the relation $f^2$ vs $\mu$ is nonlinear.

We hope our results contribute to a better understanding of polarization and transverse instabilities, which are important for the design of VCSEL's with optimized performance.

## ACKNOWLEDGMENTS

C.M. acknowledges support from the "Ramon and Cajal" Program and the Spanish Ministerio de Educaciòn y Ciencia through project FIS2005-07931-C0-03. M.S.T. acknowledges partial support of CONICET Grant No. PIP 2779 and FONCyT Grant No. 3/9598, Argentina. P.M. acknowledges support of the Fonds National de la Recherche Scientifique (Belgium) and the Interuniversity Attraction Pole Programme-Belgian Science Policy.

[1] C. J. Chang-Hasnain, J. P. Harbison, G. Hasnain, A. C. V. Lehmen, L. T. Florez, and N. G. Stoffel, IEEE J. Quantum Electron. **27**, 1402 (1991).
[2] M. Travagnin, M. P. van Exter, A. K. Jansen van Doorn, and J. P. Woerdman, Phys. Rev. A **54**, 1647 (1996); M. Travagnin, M. P. van Exter, A. K. Jansen van Doorn, and J. P. Woerdman, Phys. Rev. A **55**, 4641(E) (1997).
[3] M. Travagnin, M. P. van Exter, and J. P. Woerdman, Phys. Rev. A **56**, 1497 (1997).
[4] M. Travagnin, M. P. van Exter, and J. P. Woerdman, Phys. Rev. A **56**, 1497 (1997).
[5] G. Giacomelli and F. Marin, Quantum Semiclassic. Opt. **10**, 469 (1998).
[6] G. Giacomelli, F. Marin, M. Gabrysch, H. H. Gulden, and M. Moser, Opt. Commun. **146**, 136 (1998).
[7] K. D. Choquette, D. A. Richie, and R. E. Leibenguth, Appl. Phys. Lett. **64**, 2062 (1994).
[8] A. Valle, J. Sarma, and K. A. Shore, IEEE J. Quantum Elec-

tron. **31**, 1423 (1995).
[9] M. San Miguel, Q. Feng, and J. V. Moloney, Phys. Rev. A **52**, 1728 (1995).
[10] J. Martin-Regalado, F. Prati, M. San Miguel, and N. B. Abraham, IEEE J. Quantum Electron. **33**, 765 (1997).
[11] J. Martin-Regalado, J. L. A. Chilla, J. J. Rocca, and P. Brusenbach, Appl. Phys. Lett. **70**, 3350 (1997).
[12] J. Dellunde, M. C. Torrent, J. M. Sancho, and K. A. Shore, IEEE J. Quantum Electron. **33**, 1197 (1997).
[13] O. Buccafusca, J. L. A. Chilla, J. J. Rocca, P. Brusenbach, and J. Martin-Regalado, IEEE J. Quantum Electron. **35**, 608 (1999).
[14] S. Balle, E. Tolkachova, M. San Miguel, J. R. Tredicce, J. Martin-Regalado, and A. Gahl, Opt. Lett. **24**, 1121 (1999).
[15] M. Sciamanna, K. Panajotov, H. Thienpont, I. Veretennicoff, P. Megret, and M. Blondel, Opt. Lett. **28**, 1534 (2003).
[16] Y. H. Hong, M. W. Lee, P. S. Spencer, and K. A. Shore, Opt. Lett. **29**, 1215 (2004).
[17] M. B. Willemsen, A. S. van de Nes, M. P. van Exter, J. P. Woerdman, M. Brunner, and R. Hovel, Appl. Phys. Lett. **77**, 3514 (2000).
[18] A. Scire, J. Mulet, C. R. Mirasso, and M. San Miguel, Opt. Lett. **27**, 391 (2002).
[19] M. Yamada, IEEE J. Quantum Electron. **29**, 1330 (1993).
[20] K. Panajotov, G. Van der Sande, H. Thienpont, and I. Veretennicoff, J. Opt. Soc. Am. B **21**, 1194 (2004).
[21] G. Van der Sande, K. Panajotov, M. Peeters, I. Veretennicoff, J. Danckaert, and T. Erneux, Opt. Lett. **29**, 53 (2004).
[22] M. S. Torre, C. Masoller, and P. Mandel, Phys. Rev. A **66**, 053817 (2002).
[23] M. S. Torre, C. Masoller, P. Mandel, and K. A. Shore, IEEE J. Quantum Electron. **40**, 620 (2004).
[24] M. S. Torre, C. Masoller, and K. A. Shore, J. Opt. Soc. Am. B **21**, 1772 (2004).
[25] J. Y. Law and G. P. Agrawal, IEEE J. Quantum Electron. **33**, 462 (1997).
[26] J. Martin-Regalado, S. Balle, M. San Miguel, A. Valle, and L. Pesquera, Quantum Semiclassic. Opt. **9**, 713 (1997).
[27] M. S. Sodha and A. K. Ghatak, *Inhomogeneous Optical Waveguides* (Plenum Press, New York, 1977).
[28] B. Ryvkin, K. Panajotov, A. Georgievski, J. Danckaert, M. Peeters, G. Verschaffelt, H. Thienpont, and I. Veretennicoff, J. Opt. Soc. Am. B **16**, 2106 (1999).
[29] T. Ackemann and M. Sondermann, Appl. Phys. Lett. **78**, 3574 (2001).
[30] M. Sondermann, M. Weinkath, and T. Ackemann, IEEE J. Quantum Electron. **40**, 97 (2004).
[31] J. Mulet, C. R. Mirasso, and M. San Miguel, Phys. Rev. A **64**, 023817 (2001).
[32] C. Masoller, M. S. Torre, and P. Mandel, J. Appl. Phys. **99**, 026108 (2006).
[33] O. Carroll, Y. Tanguy, J. Houlihan, and G. Huyet, Opt. Commun. **239**, 429 (2004).